international journal of aeroacoustics volume 9 · number 3 · 2010 – pages 307–327

One, no one and one hundred thousand methods for low-speed fan noise prediction

Damiano Casalino*[,1], Stephane Moreau†[,2], Michel Roger‡[,3]

[1]*CIRA, Italian Aerospace Research Center, Capua, 81043, Italy*

[2]*VALEO Motors and Actuators, La Verrière, 78321, France*

[3]*Ecole Centrale de Lyon, Ecully, 69134, France*

Received March 5, 2009; Revised February 25, 2010; Accepted March 1, 2010

ABSTRACT

A hybrid CFD/integral approach is used to predict the noise spectrum of a real automotive fan cooling system. The tonal and broadband noise spectral components, mainly due to the coherent and random part, respectively, of the unsteady pressure fluctuations induced by the rotor-wake/stator-vane interaction, are computed by applying a Ffowcs-Williams & Hawkings acoustic analogy to the wall pressure field provided by a transient Reynolds-averaged Navier-Stokes simulation, with superimposed random fluctuations computed through a stochastic method. The RANS turbulent quantities are used to generate solenoidal stochastic velocity fluctuations that contribute to define the right-hand side of a Poisson equation for the pressure perturbation. The Poisson equation is cast into a boundary integral equation and solved by means of a boundary element method. The noise spectra at different angles with respect to the fan axis are computed and compared with available experimental data.

NOMENCLATURE

B^R	Number of rotor blades
B^S	Number of stator blades
E	Turbulent kinetic energy spectrum
F	Pressure force on the surface element
J	Element transformation Jacobian
K	Turbulent kinetic energy
L_t	Integral length scale
M	Source Mach number
$\mathcal{N}$	Element shape functions

* Senior Research Engineer, Rotorcraft Aerodynamics and Aeroacoustics Laboratory.

† Senior Research Engineer and R&D Manager, Engine Cooling Fan Systems Core Competencies Group.

‡ Professor of Aeroacoustics, Fluid Mechanics and Acoustics Laboratory.

$\mathcal{P}$	Probability density function
Q	Poisson equation source term
T_{ij}	Reynolds tensor
U	Reynolds-averaged velocity
V	Surface velocity
c	Speed of sound
k	Vortical wavenumber ($k = \|\mathbf{k}_n\|$)
k_e	Maximum kinetic energy wavenumber
k_v	Kolmogorov wavenumber
$\hat{\mathbf{n}}$	Normal unit vector
p	Pressure
$\hat{\mathbf{r}}$	Radial unit vector
$\hat{u}_n$	Magnitude of the velocity mode
u'	Turbulent velocity fluctuation

Subscripts

a	Atmospheric ambient quantities
M	Projection on the source velocity direction
n	Projection on the surface normal direction
r	Projection on the source-to-observer direction
ret	Retarded-time evaluation

Conventions

BEM	Boundary Element Method
BPF	Blade Passage Frequency
BPP	Blade Passage Period
CAA	Computational Aero-Acoustics
FW-H	Ffowcs-Williams & Hawkings
RANS	Reynolds-Averaged Navier-Stokes
SGNR	Stochastic Noise Generation and Radiation
SPL	Sound Pressure Level

Symbols

α_n , ϕ_n, θ_n, ψ_n, ω_n, SNGR	random quantities
$\Delta\Psi_i$	Angular stagger of the i-th blade
δ_{ij}	Kronecher symbol
ϵ	Turbulent dissipation
μ_t	Turbulent viscosity
ν	Laminar kinematic viscosity
ω	Specific turbulence dissipation rate
ρ	Density
σ_n	Velocity fluctuation unit vector
τ	Source emission time
τ_i	Time lag of the i-th blade
ξ, η, ζ	Element local coordinates

Superscripts

$'$	Perturbation quantities
$\cdot$	Time derivative
$\bar{}$	Reynolds-average operator

1. INTRODUCTION

The noise generated by a fan system mounted on a cooling module is characterized by a broadband spectrum from which tonal components at the BPF harmonics arise. The contribution of the broadband and tonal components to the integrated noise levels can be of the same order. For this reason, both these components are to be taken under control in the design process of a new automotive engine cooling fan system.

The prediction of the tonal noise components can be easily accomplished within computational times of industrial utility by performing unsteady RANS computations with the same space-time resolution required by accurate performance analysis. The robustness reached by commercial CFD tools on one side, and the growing performances of low-cost computational systems on the other side, permit to attain full 2π grid converged transient solutions in reasonable times.[1] During the preliminary design phase, when several simulations are required for different configurations and operating conditions, some simplification can be made in order to reduce the time for the numerical analysis. One of these consists in simulating only one blade passage by supposing an equal number of rotor blades and stator vanes and using periodicity boundary conditions. This is the case, for instance, of the RANS solution used in this paper computed in 2004[2] and here used as a support for the development of the broadband noise method. Another very common simplification made for low-speed fans consists in solving incompressible RANS equations with effcient numerical schemes. A pure hydrodynamic wall pressure field is not consistent with a FW-H acoustic analogy. However, since the dipole sources at the lowest BPFs are acoustically compact, the use of incompressible CFD solutions for FW-H far-field noise is practically permitted. Hence, the unsteady RANS solution coupled with a FW-H acoustic analogy noise extrapolator constitutes the "one" method for low-speed fan tonal noise prediction.

The prediction of the broadband noise components through CFD approaches is a quite more challenging task. LES computations of realistic turbomachinery configurations with accurate space-time statistical correlation properties have been accomplished only in excellence research centers[3] and are not easily repeatable in industrial environments. Even for low-speed cooling fans, for which fast incompressible solvers can be used, the situation is not better and only few solutions are reported in the literature. For this reason, the LES approach is still the "no one" method for low-speed fan broadband noise prediction.

The only viable solution for the prediction of the broadband noise prediction of cooling fan systems, as well as other rotating devices like wind turbines and helicopter blades, consists in adapting theoretical models developed for two-dimensional airfoils to the rotating blades through a strip approach. This is the method used in the past for helicopter trailing-edge noise,[4] helicopter ingested turbulence noise[5] and, more recently,

low speed fan trailing- and leading-edge noise.[6] Theoretical models of trailing- and leading-edge noise of two-dimensional airfoils have been developed mainly in the seventies[7–13] and even more recently.[6,14–16] The main differences between all these approaches are related to the near field statistical quantity used to characterize the noise generation process (velocity or wall pressure power spectral density and correlation lengths), and on the method used to extrapolate the near-field statistics to the far-field noise power spectral density (tailored Green's functions or singulary distribution methods). The theoretical model recently developed by Roger and Moreau,[6,17] by following the approach outlined by Amiet,[9,10] predicts accurately the high-frequency noise levels generated by the trailing-edge of a low-speed axial fan, provided that the proper wall pressure power spectral density, spanwise wall pressure correlation and turbulent convection velocity are used. These quantities are extracted from measurements undertaken on two-dimensional airfoils at different angles of attack in the free-jet of an anechoic wind tunnel.[18] This theoretical method, together with the acquired expertise in the selection of the proper airfoil statistical data set, constitutes the VALEO "one method" for low-speed fan broadband noise prediction.

An interesting alternative to the measurements of wall pressure or other near-field statistics consists in using the mean flow and averaged turbulence quantities provided by a RANS computation to generate stochastic velocity fluctuations. These are combined in the right-hand side of linearized equations and used to compute the perturbation field. A great variety of stochastic approaches is available in the literature,[19–22] depending on the technology field, the system of linearized equations used to describe the perturbation field, the way how the kinetic energy is distributed on the wavenumber energy spectrum, the way how the space correlation lengths are extracted from the RANS solution and translated into the stochastic model. Therefore, the stochastic methods, those already proposed and those not yet proposed, belong to the category of "one hundred thousand methods" for a wide class of aeroacoustic applications, included the prediction of low-speed fan broadband noise.

The main objective of this paper is to report on a newly developed methodology for hybrid RANS/FW-H tonal and broadband noise predictions based on the use of a stochastic approach to generate wall pressure fluctuations from a RANS solution. The original contribution of this work consists in the fact that the stochastic method is not used to generate source terms for a set of perturbation equations, but it is used to compute wall pressure fluctuations that are added to the wall pressure fluctuations provided by RANS and used to perform FW-H noise computations. The method is described in section (II) and used to generate the results presented in section (IV). Few underlying elements about the computational tools involved in the prediction chain are reported in section (III). Finally, the main conclusions of the present study and the foreseen improvements are drawn in section (V).

2. STOCHASTIC WALL PRESSURE FLUCTUATIONS MODEL

As shown by Ffowcs-Williams,[23, 24] the proper way to describe the statistical behaviour of wall pressure fluctuations beneath a turbulent boundary layer in the whole wavenumber/frequency regime is through a Curle-Lighthill[25] acoustic analogy approach that

permits to take into account the flow compressibility effects. For turbulent velocity fluctuations with subsonic phase speed, say $\omega / k < c_a$, with ω and k denoting the radian frequency and space wavenumber of a convected vortical perturbation, a dimensional analysis suggests that a Poisson equation for the pressure perturbation can be used in alternative to the Lighthill's equation. In other words, the phase shift between the pressure perturbations induced by vortical fluctuations with subsonic phase speed can be neglected. This hypothesis has been used in the past to develop models for the wavenumber-frequency spectrum of wall pressure fluctuations beneath a turbulent boundary layer.[26–28]

As a first attempt to generate wall pressure fluctuation starting from a stochastic representation of the velocity field, in this paper we adopt a pure hydrodynamic model for the pressure fluctuations by solving the following Poisson equation:

$$\nabla^2 p' = -2\rho_a \frac{\partial U_i}{\partial x_j}\frac{\partial u_j'}{\partial x_i} - \rho_a \frac{\partial u_i'}{\partial x_j}\frac{\partial u_j'}{\partial x_i} - \frac{\partial^2 T_{ij}}{\partial x_i \partial x_j} \equiv Q(\mathbf{x},t), \tag{1}$$

where U_i is the Reynolds-averaged flow velocity component, μ_i' is the turbulent flow velocity component and $T_{ij} \equiv -\rho_a \overline{u_i' u_j'}$ is the Reynolds stress tensor. Following a standard RANS approach, T_{ij} can be modeled as:

$$T_{ij} = \mu_t \left(\frac{\partial U_i}{\partial x_j} + \frac{\partial U_j}{\partial x_i} \right) - \frac{2}{3}\rho_a K \delta_{ij}, \tag{2}$$

where K denotes the turbulent kinetic energy per unit of volume and μ_t is the turbulent viscosity.

In order to generate the velocity fluctuations required by the right-hand side of Eq. (1), the approach outlined in the SNGR model[19,20] can be used. As a first step, the velocity fluctuation can be defined as a sum of Fourier components, i.e.:

$$\mathbf{u}'(\mathbf{x},t) = 2\sum_{n=1}^{N} \hat{u}_n \cos\{\mathbf{k}_n \cdot (\mathbf{x} - \mathbf{U}t) + \psi_n + \omega_n t\}\boldsymbol{\sigma}_n, \tag{3}$$

where $\hat{u}_n, \psi_n$, and $\boldsymbol{\sigma}_n$ are magnitude, phase and direction of the n^{th} Fourier component, respectively. Each Fourier mode is convected at the local mean flow velocity $\mathbf{U}$. The scalar product $\mathbf{k}_n \cdot \mathbf{U}$ accounts for the time variation of the velocity fluctuation, together with the characteristic radian frequency ω_n. Assuming incompressibility, the zero divergence condition applied to Eq. (3) results in the relationship $\mathbf{k}_n \cdot \boldsymbol{\sigma}_n = 0$, stating that the wave vector is perpendicular to the velocity vector.

By supposing that the turbulent flow field is isotropic, the magnitude of the n^{th} Fourier mode is related to the mono-dimensional energy spectrum $E(k)$ by the expression $\hat{u}_n = \sqrt{E(k_n)\Delta k_n}$, where k_n and Δk_n are the wavenumber and the

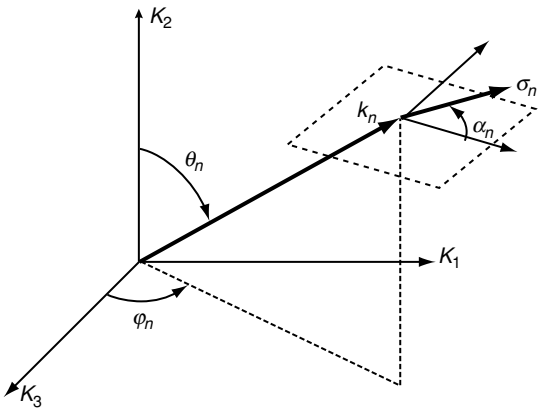

Figure 1: Schematic view of the wave vector k_n and velocity direction vector $\boldsymbol{\sigma}_n$.

corresponding band of the n^{th} mode. A common practice consists in using the Von Kármán-Pao isotropic turbulence spectrum, i.e.:

$$E(k) = \frac{A(2/3)(K/k_e)(k/k_e)^4 \exp[-2(k/k_\eta)]}{[1+(k/\boldsymbol{k}_e)^2]^{17/6}}, \tag{4}$$

where A is a is a numerical constant, k_e is the wavenumber of maximum energy and $k_\eta = \epsilon^{1/4}\nu^{-3/4}$ is the Kolmogorov wavenumber. The constants A and k_e can be determined by equating the integral energy and the integral length scale derived from Eq. (4) to the RANS quantities K and $L_T = u'^3/\epsilon$, respectively, $u' = \sqrt{2K/3}$ being the isotropic turbulent velocity. This provides $A \simeq 1.453$ and $k_e = 0.747/L_T$.

The stochastic velocity perturbation field can be now generated by choosing probability density functions for all the random variables involved in Eq. (3). These are: the angles ϕ_n and θ_n defining the direction of the wave vector $\mathbf{k}_n$, as sketched in Fig. (1), the angle α_n defining the direction of the unit vector $\boldsymbol{\sigma}_n$ in a plane orthogonal to $\mathbf{k}_n$, the phase ψ_n and the radian frequency ω_n. By requiring that the wave vector is uniformly distributed in the three-dimensional wavenumber space provides the following probability densities:

$$\mathcal{P}(\phi_n) = (2\pi)^{-1}, \quad \text{with} \quad 0 \le \phi_n \le 2\pi \tag{5}$$

$$\mathcal{P}(\theta_n) = \sin(\theta_n)/2, \quad \text{with} \quad 0 \le \theta_n \le \pi \tag{6}$$

Analogously, by supposing that the $\boldsymbol{\sigma}_n$ vector is uniformly distributed in the plane normal to $\mathbf{k}_n$ yields:

$$\mathcal{P}(\alpha_n) = (2\pi)^{-1}, \quad \text{with} \quad 0 \le \alpha_n \le 2\pi. \tag{7}$$

The phase ψ_n is also supposed to be uniformly distributed in the 2π range, i.e.:

$$\mathcal{P}(\psi_n) = (2\pi)^{-1}, \quad \text{with} \quad 0 \leq \psi_n \leq 2\pi. \tag{8}$$

Finally, the radian frequency is supposed to have a Gaussian variation around a mean value, i.e.:

$$\omega_n = u' k_n (1 + \varrho \Gamma_n), \tag{9}$$

where $\varrho = 0.1$ is arbitrarily chosen and Γ_n is a random variable with a unit variance Gaussian distribution.

In order to force the space correlation into the stochastic velocity fluctuations, a zero-order approach is used, which consists in assuming full correlation between sources located in the same cell of a constant Cartesian mesh of cell size $\langle l_T \rangle$ equal to the average value over the source region of the geometric man value of the turbulent correlation length:

$$\langle l_T \rangle = \left\langle \sqrt{\prod_{i=1}^{3} |T_{ii}/\rho_0|}/\epsilon \right\rangle$$

Random quantities are generated independently for each Cartesian cell and attributed to the encompassed source points.

A formal solution to the Poisson equation can be derived as asymptotic limit for $c_0 \to \infty$ of Curle's integral formula,[25] i.e.:

$$2\pi p'(\mathbf{x}, t) - \iint_S \frac{p' \hat{r}_n}{r^2} \mathrm{d}S_y = \iiint_V \frac{Q(\mathbf{y}, t)}{r} \mathrm{d}V_y, \tag{10}$$

where $r = |\mathbf{x} - \mathbf{y}|$ and $\hat{r_n} = \hat{\mathbf{n}} \cdot (\mathbf{x} - \mathbf{y}) / r$, with $\hat{\mathbf{n}}$ pointing into the flow. This integral equation is solved at each time step by using a BEM approach based on iso-parametric elements of the first order and Gaussian quadrature.[29] The left-hand side matrix is computed only at the first time step and used for the whole transitory.

The generation of the stochastic source term for Eq. (1) and its numerical solution providing the wall pressure stochastic field is accomplished through the following steps.

- A transitory $K - \omega$ RANS solution covering one blade passage is imported and used to compute the time-Fourier coeffcients of the wall pressure fluctuations. This allows, in the final stage of the present process, to generate transient pressure fields randomly perturbed at a smaller sampling time in order to meet required frequency specifications in the noise spectral analysis. In addition, the relative velocity, turbulent kinetic energy and dissipation $\epsilon = 0.09 K\omega$ are averaged over the BPP. The average velocity provides the convection velocity at each point of the computational mesh, as required by Eq. (3), whereas the average turbulent quantities are used to define the energy spectrum and turbulent velocity u' at each point of the computational mesh.

- An active portion of the whole discretized volume in which the source term of Eq. (1) is supposed to be non-zero is defined by specifying a cut-off distance from the wall. A list of nodes belonging to the source volume is generated at the beginning of the computation and used throughout the transient simulation.
- For each node belonging to the active volume, once specified the required number N of Fourier modes, the random sets ϕ_n , ψ_n , α_n an and θ_n are generated using standard algorithms provided by the Numerical Recipes library.[30] The wavenumber space is discretized in N samples with a logarithmical distribution from the minimum value k_1 to the maximum value k_N , chosen as the minimum value of k_e and the maximum value of k_v in the whole field, respectively, i.e.:

$$k_n = \exp\left\{\log(k_1) + \frac{n-1}{N-1}[\log(k_N) - \log(k_1)]\right\}, \quad \text{with} \quad n = 1..N \tag{11}$$

- For each node belonging to the active volume, the derivatives $\partial U_i / \partial x_j$ and $\partial^2 T_{ij} / \partial x_i \partial x_j$ are computed by using polynomial shape functions in an unstructured mesh framework. Conversely, the derivatives of the perturbation velocity are computed analytically from Eq. (3).
- A new time step and a final transient time are defined in order to meet specific requirements in terms of maximum frequency and frequency band. At each time step, the right-hand side of Eq. (1) is computed and used to solve Eq. (10). The random wall pressure solution is then added to the RANS wall pressure solution recovered by inverse Fourier transformation from the coeffcients computed at the beginning of the computation, as outlined at the first item.

3. BUILDING ELEMENTS OF THE CFD/FW-H APPROACH

3.1. Fan system, CFD mesh topology and RANS solution

The fan cooling system addressed in this paper combines an ultra compact fan developed in 2003 by VALEO with a long-duration and effcient stator.[31] A view of the fan is shown in Fig. (2(a)). It has 9 blades of 0.15 m tip-radius, with a non-uniform circumferential distribution in order to reduce the level of the "rotor-locked" tonal noise peaks. A view of the stator is shown in Fig. (2(b)). It has 10 blades with a uniform circumferential distribution. The CFD results herein used as support for the development of the stochastic method have been computed in 2004[2] by using a PC with quad core processor. At that time a fully converged solution was easily achievable by simulating only one single blade passage and using periodicity boundary conditions. Therefore, a uniform rotor blade distribution was assumed and a 9/9-blades rotor/stator system (one-to-one) was simulated. However, as described in subsection (III.B), the different rotor/stator blade count is partially restored in the aeroacoustic computation by forcing a time lag in the noise computation from each blade.

Both the rotor and the stator grid topologies corresponds to automatic block-structured grid templates in use at VALEO. The rotor grid, shown in Fig. (3(a)), includes the actual blade and tip clearance geometry and, downstream, the motor or

(a) Fan rotor view (b) Support-stator view

Figure 2: VALEO engine cooling fan system.

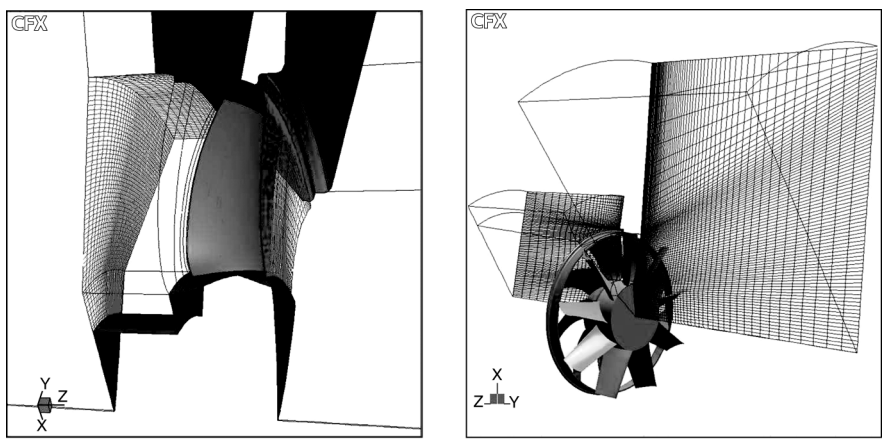

(a) Rotor view (b) Support-stator view

Figure 3: Multi-block structured grid used for the CFD simulation.

torque meter blockage. Only the swirling effect of the ribs within the fan hub is neglected. The stator grid, shown in Fig. (3(b)), has some key features that allow to describe properly the unsteady wake/stator interaction mechanism.[32,33] The whole computational mesh involves about one million nodes and permits to resolve properly the boundary layer at the Reynolds number of interest. This type of simulation and the model size have been validated on several engine cooling devices with both integral performances and detailed flow measurements.[34,35]

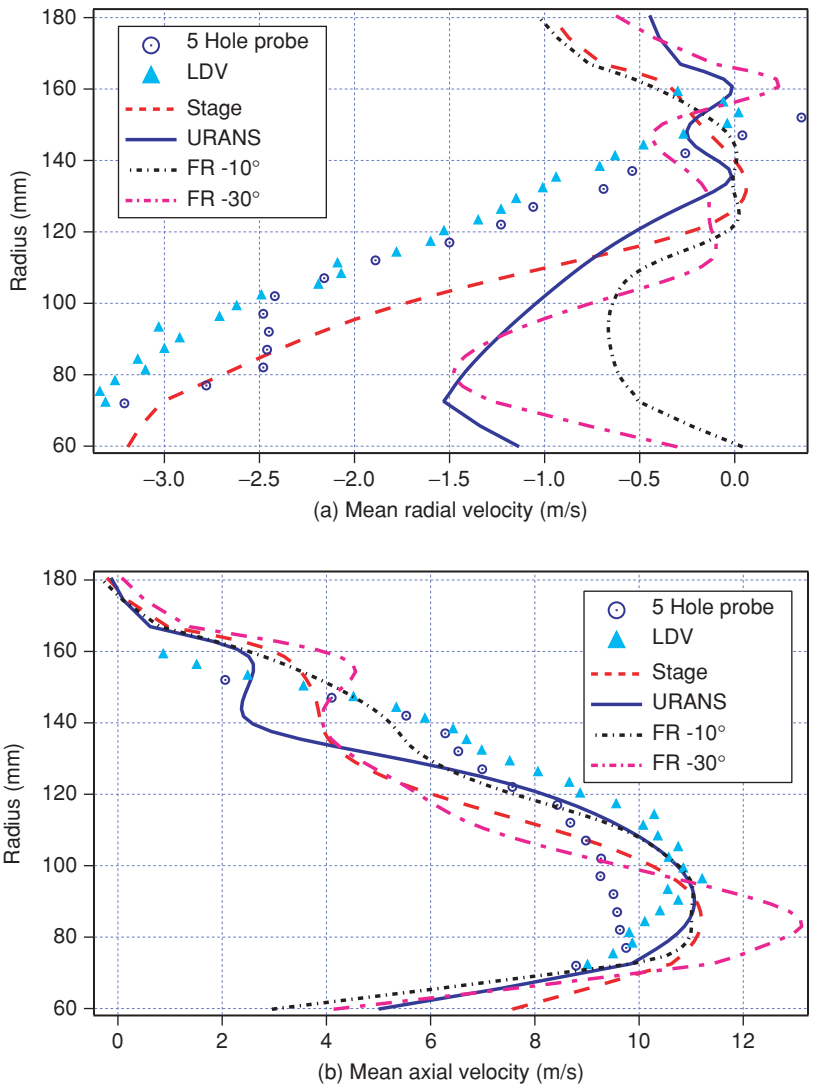

Figure 4: Comparison between computed (blue line) and measured (symbols) velocity profiles 0.04 m downstream of the stator vanes.

The commercial software CFX-TASCflow™ has been used to solve the incompressible unsteady RANS equations based on a two-equation $K-\omega$ SST closure model.[36] The resulting system of conservative equations is discretized in space by a second order upwind scheme for the convective terms and second order central differences for all other spatial derivatives. A second order implicit scheme, with a dual-time stepping approach, has been used to advance the solution in time. The simulation

involves 32 physical transient steps per BPP, with 20 pseudo-time sub-iterations every transient step. A number of 10 full BPPs are computed and only the last one is used for the present numerical study. The transient solution is converged to similar accuracy both in space and time, providing a confident level of accuracy in featuring the basic unsteady flow mechanisms. The resulting integral pressure rise with flow rate is found to compare favorably with available experimental measurements.[1] Moreover, as shown in Fig. (4), the axial and radial velocity profiles at 0.04 m downstream of the stator vanes are shown to lie within the spread-out of the experimental data observed in both the five-hole probe and LDV measurements. Only the radial component is found to be underestimated at the hub, which could be explained by the lack of fan ribs in the numerical simulation. In fact, these ribs act as centrifugal pumps which trigger a strong flow suction through the electrical motor.

3.2. FW-H and BEM integral methods

Both the FW-H and the BEM solvers used in the present work are part of a library of methods recently developed by the first author and denominated *OptydB*. In this library the aeroacoustic methods developed in the past, for both frequency-domain analysis (GFD[37]) and time-domain analysis (Foxwhawk[38]), plus a standard FEM solver for the convected Helmholtz equation, have been merged by sharing most of the computational and numerical features. These include: input/output management, connectivity graphs generation, automatic mesh partitioning and parallel distribution of the computation, surface/volume integration, polynomial shape computation for generic surface/volume elements, linear system solver, advanced searching algorithms used, for instance, in the projection of the solution from one mesh to another.

The FW-H solver is based on a retarded-time penetrable formulation,[39,40] but solved in a forward-time framework. For the present low-speed fans, the quadrupole noise is ignored and only the thickness and loading noise contributions are calculated, that read:
Thickness noise:

$$4\pi p'_T(\vec{x},t) = \iint_S \left[\frac{\rho_a\left(\dot{V}_n + V_{\dot{n}}\right)}{r\left(1-M_r\right)^2}\right]_{\text{ret}} \mathrm{d}S_y + \iint_S \left[\frac{\rho_a V_n\left(r\dot{M}_r + c_a\left(M_r - M^2\right)\right)}{r^2\left(1-M_r\right)^3}\right]_{\text{ret}} \mathrm{d}Sy, \quad (12)$$

where $r = |\mathbf{x} - \mathbf{y}(\tau)|$ is the source-to-observer distance, $\overrightarrow{M}$ of magnitude M is the Mach number vector of a source point on the blade surface S, which moves with an outward normal velocity V_n. The dotted quantities denote time derivative with respect to the source time τ. M_r is the relative Mach number, i.e., the projection of $\overrightarrow{M}$ in the observer direction.
Loading noise:

$$4\pi p'_L(\vec{x},t) = \frac{1}{c_a}\iint_S \left[\frac{\dot{F}_r}{r(1-M_r)^2}\right]_{\text{ret}} \mathrm{d}S_y + \iint_S \left[\frac{F_r - F_M}{r^2(1-M_r)^2}\right]_{\text{ret}} \mathrm{d}S_y$$

$$+\frac{1}{c_a}\iint_S \left[\frac{F_r\left(r\dot{M}_r + c_a(M_r - M^2)\right)}{r^2(1-M_r)^3}\right]_{\text{ret}} \mathrm{d}S_y, \tag{13}$$

where $\overrightarrow{F}$ is the pressure force acting on the surface S, and F_M is this force projected in the source movement direction.

The forward-time formulation enables concurrent CFD/FW-H simulations. For the sake of the present work the code is only used to post-process transient wall pressure fields extracted from CFX-TASCflow™ solution previously computed. Only linear effects due to the blade thickness and loading are computed, and nonlinear volume quadrupoles are neglected on the basis of small blade tip Mach number. Integrations on rotating and fixed elements are carried out independently, allowing a separation of the rotor and stator noise contributions. For one single blade, the integration surface consists of about 24×10^3 elements. However, due to the serious computational constraints of the BEM approach, a grid clustering technique has been used to reduce the number of element by a factor 4.

Transient CFD data covering one BPP (19 multi-block structured files) are cyclically imported in order to simulate several blade passages. The rotation frequency is 50 Hz, corresponding to a blade passing frequency of 450 Hz. The periodic B-blades configuration is automatically generated by the FW-H solver before integrations. The actual blade counts ($B^R = 9$ and $B^S = 10$) is automatically recovered by forcing into the forward-time formula the following time lag for the i-th rotor blade:

$$\tau_i = (i-1)\frac{\mathrm{sgn}(\Omega_z)}{\mathrm{BPF}}\frac{B^S - B^R}{B^S}, \tag{14}$$

where z is the axial direction oriented from the stator to the rotor. The same time lag, but changed of sign is used for the stator blades. This expression accounts for a uniform circumferential blade distribution. In order to account for a non uniform circumferential distribution of the fan blades, as for the present configuration, a corrective term can be added to Eq. (14), say:

$$\tau_i^\star = \frac{\mathrm{sgn}(\Omega_z)\Delta\Psi_i B^R}{2\pi\mathrm{BPF}}, \tag{15}$$

where $\Delta\Psi_i$ (rad) is the angular stagger of the i-th rotor blade from its uniform angular location.

The acoustic signals are computed at a distance of 1 m from the fan rotation center and every 30 deg from the fan axis, from 0 to 90 deg.

The stochastic wall pressure computation is carried out by sampling one full rotation period into 400 time steps, providing a Nyquist frequency of 10 kHz. The stochastic fluctuations are added to the RANS fluctuations that are sampled on the new time series through an inverse Fourier transform. The rotor and stator FW-H computations are carried out separately and are successively added. However, in order to force statistical uncorrelation, the rotor and stator signals are extended over 100 rotation periods by concatenating 100 computed signals, each one starting from a random multiple of the BPP. The new rotor and stator signals are finally added and used to perform a spectral analysis. This is carried out by requiring a frequency band of 4 Hz and a number of 20 spectral averages, and by letting the spectral tool computing the proper time windows overlapping.

The BEM solver used to solve Eq. (10) is based on a standard isoparametric approach. The surface is discretized into a number N_e of triangular or quadrilateral elements and the surface integral is decomposed into a summation over elementary integrals,i.e.:

$$\iint_S \frac{p'\hat{r}_n}{r^2} = \sum_{n=1}^{N_e} \int_{-1}^{1}\int_{-1}^{1} p'(\xi,\eta) \frac{\hat{\mathbf{n}}(\xi,\eta)\cdot(\mathbf{x}-\mathbf{y}(\xi,\eta))}{\left|\mathbf{x}-\mathbf{y}(\xi,\eta)\right|^3} J^n(\xi,\eta)\,\mathrm{d}\xi\,\mathrm{d}\eta, \tag{16}$$

where $J^n(\xi, \eta)$ is the Jacobian of the transformation of the generic element n into the sample quad element. The isoparametric approach consists in using the function basis that transforms the generic element into the sample element to model p' inside the element, i.e.:

$$p'(\xi,\eta) = \sum_{j=1}^{N_v} p'_j \mathcal{N}_j(\xi,\eta) \quad \text{and} \quad \mathbf{y}(\xi,\eta) = \sum_{j=1}^{N_v} \mathbf{y}_j \mathcal{N}_j(\xi,\eta), \tag{17}$$

where $\mathcal{N}_j(\xi, \eta)$ are the shape functions of the element n, N_v is the number of vertices of the element, p'_j are the values of p' at the vertices and $\mathbf{y}_j$ are the coordinates of the vertices. Eq. (16) can be now substituted into Eq. (10) that can be collocated at each point $\mathbf{x}_i$ of the discretized surface, i.e.:

$$\begin{aligned} p'_i - \sum_{n=1}^{N_e}\sum_{j=1}^{N_v} p'_j \int_{-1}^{1}\int_{-1}^{1} \mathcal{N}_j^n(\xi,\eta) \frac{\hat{\mathbf{n}}(\xi,\eta)\cdot(\mathbf{x}_i-\mathbf{y}(\xi,\eta))}{\left|\mathbf{x}_i-\mathbf{y}(\xi,\eta)\right|^3} J^n(\xi,\eta)\,\mathrm{d}\xi\,\mathrm{d}\eta = \\ \sum_{k=1}^{N_k} \int_{-1}^{1}\int_{-1}^{1}\int_{-1}^{1} \frac{Q(\mathbf{y}(\xi^\star,\eta^\star,\zeta^\star),t)}{\left|\mathbf{x}_i-\mathbf{y}(\xi^\star,\eta^\star,\zeta^\star)\right|} J^k(\xi^\star,\eta^\star,\zeta^\star)\,\mathrm{d}\xi^\star\,\mathrm{d}\eta^\star\mathrm{d}\zeta^\star, \end{aligned} \tag{18}$$

where N_k is the number of active source cells close to the surface. The double summation over all the elements and, for each element, over all the vertices, can be replaced by a double summation over all the surface nosed N_n and, for each nodes, over all the adjacent elements N_e^j, i.e.

$$p'_i - \sum_{j=1}^{N_n} p'_j \sum_{n=1}^{N_e^j} \int_{-1}^{1}\int_{-1}^{1} \mathcal{N}_j^n(\xi,\eta) \frac{\hat{\mathbf{n}}(\xi,\eta)\cdot(\mathbf{x}_i - \mathbf{y}(\xi,\eta))}{\left|\mathbf{x}_i - \mathbf{y}(\xi,\eta)\right|^3} J^n(\xi,\eta)\,\mathrm{d}\xi\,\mathrm{d}\eta = \sum_{k=1}^{N_k} \int_{-1}^{1}\int_{-1}^{1}\int_{-1}^{1} \frac{Q(\mathbf{y}(\xi^\star,\eta^\star,\zeta^\star),t)}{\left|\mathbf{x}_i - \mathbf{y}(\xi^\star,\eta^\star,\zeta^\star)\right|} J^k(\xi^\star,\eta^\star,\zeta^\star)\,\mathrm{d}\xi^\star\,\mathrm{d}\eta^\star\mathrm{d}\zeta^\star, \quad \text{for} \quad i = 1..N_n \tag{19}$$

Finally, evaluating the surface and volume integrals by Gaussian quadrature yields a linear system with full $N_n \times N_n$ matrix that can be solved for a different right-hand sides at each time step by using an iterative solver. The present computations have been carried out on a NEC-TX7 computer by sharing the computational transient steps among 16 processors. Due to the prohibitive computational times and core memory occupation required by the original problem, a grid clustering technique has been used to reduce the number of element by a factor 4. Then each time step was converged over 2000 iterations reaching a relative error reduction of about 10^{-5} and requiring about 4 hours.

4. NOISE RESULTS AND DISCUSSION

In this section some preliminary results are presented in order to show the potentialities of the stochastic method proposed and its limits of applicability. Only the rotor configuration with a uniform circumferential blade spacing has been considered.

Fig. (5) shows the sound pressure level spectra at four observation angles generated by the stator, the rotor and their combination. At $\theta = 0$ deg the stator contribution is negligible and this is a well known property of the uneven blade count, 9-to-10 in the present case, that is recovered by forcing a time lag into the FW-H computation. Conversely, the rotor noise spectrum, as well the overall one, exhibits quasi-tonal peaks at harmonics of the BPF, broadband components at frequencies higher then 1 kHz. This pattern is the same at all the observation angles, with slight variation of the broadband noise levels and strong variation of the tonal peak levels. It is interesting to observe that the BPF harmonic (450 Hz), sufficiently away from the fan axis, is strongly affected by the stator contribution. Conversely, the 2nd harmonic peak (900 Hz) is mainly affected by the rotor contribution. Finally, when the stator and rotor tonal contribution are of the same order, a partial phase cancelation may occur, providing lower overall peak values. The peak sound pressure levels at the first three BPFs are collected in table (1).

All the noise spectra reported in Fig. (5) exhibit the same high frequency broadband spectral behavior: a bump emerging from the background noise at frequency higher than 1 kHz and extending over 8 kHz. This is the noise contribution generated by the stochastic model. The spectral bump, in fact, is a sort of image in the frequency space of the turbulent kinetic energy spectrum $E(k)$ in the wavenumber space. For the present case, the wavenumber of maximum energy at the field point where the kinetic energy is maximum is $k_e = 3.5 \cdot 10^3\ \mathrm{m}^2/\mathrm{s}^2$. Such a high value results in high frequencies stochastic fluctuation due to fine turbulence with very short integral scales. In other words, the present RANS-based stochastic model is not able to predict stochastic phenomena of larger integral scale such as, for instance, the spanwise modulation of the rotor wake impinging on the stator leading edge.

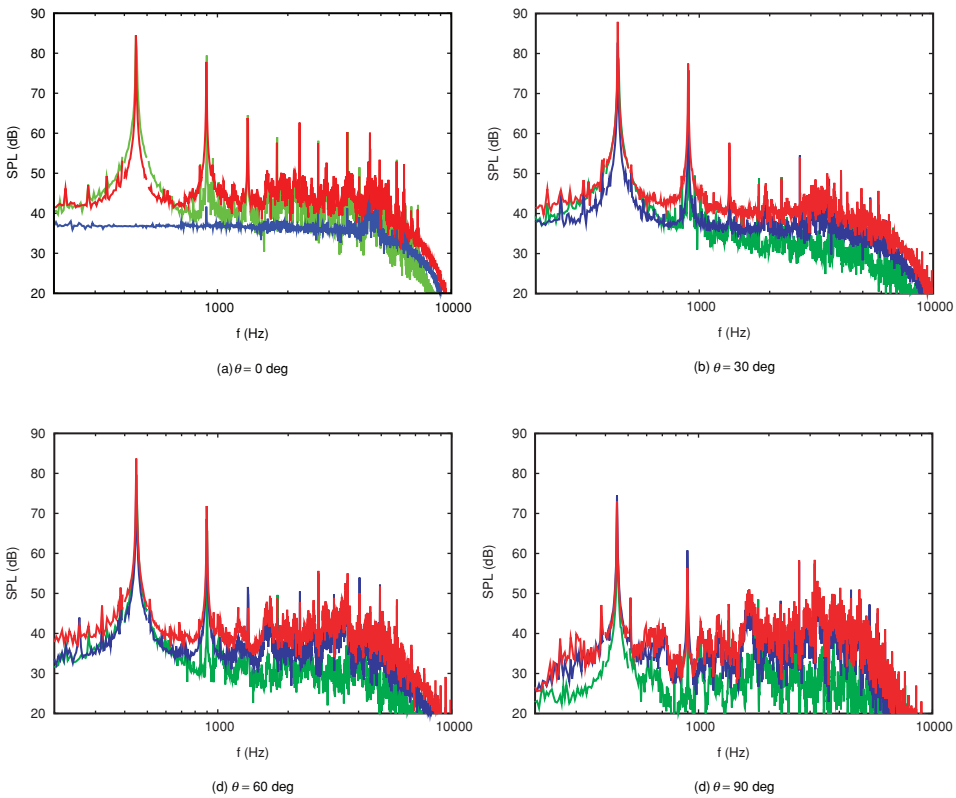

Figure 5: Sound pressure levels at different angles (integration band 4 Hz, $p_{\text{ref}} = 2\mu$ Pa). Blue: stator contribution, green: rotor contribution, red: overall.

Table 1: BPF sound pressure levels ($p_{\text{ref}} = 2\mu$ Pa) for the rotor, stator and rotor-stator combined contributions.

θ(deg)	BPF	Rotor (dB)	Stator (dB)	Overall (dB)
0	1	84.4	37.2	84.5
0	2	79.4	37.1	77.8
0	3	64.5	36.7	63.8
30	1	79.3	82.7	87.9
30	2	75.8	68.3	77.5
30	3	54.2	51.1	57.7
60	1	72.9	79.7	83.7
60	2	65.7	68.6	71.8
60	3	49.8	51.6	46.3
90	1	59.8	74.5	73.0
90	1	56.3	60.8	56.3
90	1	46.9	43.3	47.7

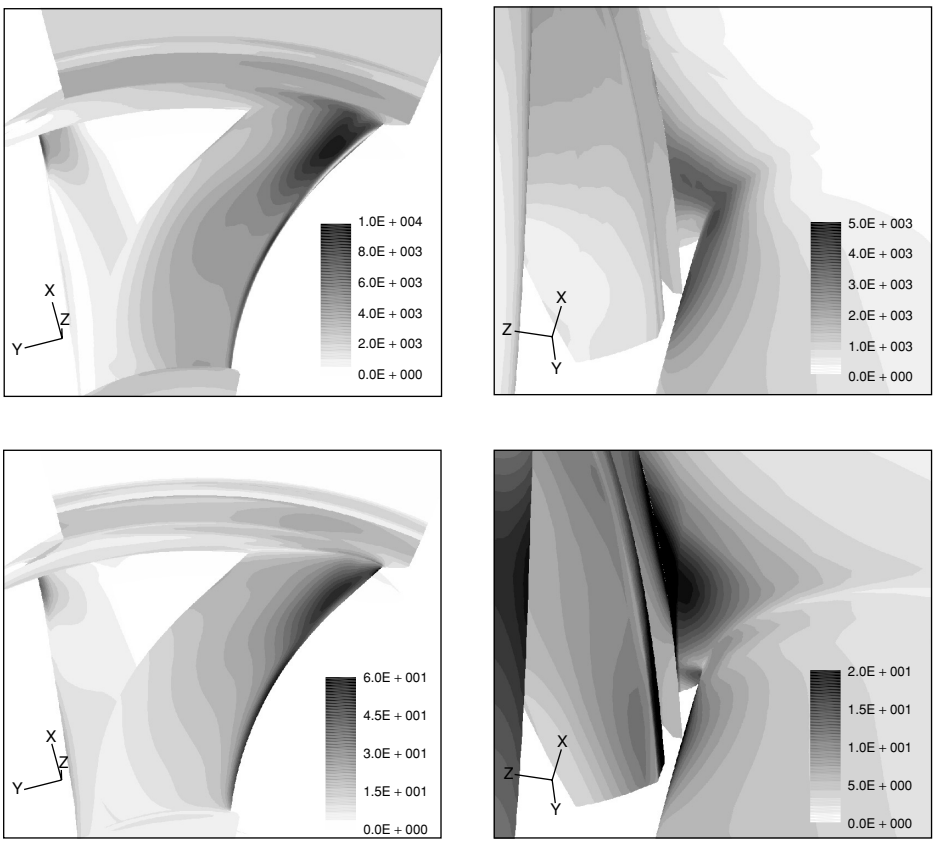

Figure 6: Distribution of the root-mean-square pressure (top) and turbulent kinetic energy (bottom) on the rotor and stator surfaces. Quantities in SI units. Rotor view on the left and stator view on the right.

Fig. (6) shows contour plots of the stochastic root-mean-square pressure and RANS kinetic turbulent energy on surface of the blades. The kinetic turbulent energy results from a wall function approach that permits to reduce the size of the first cell normal to the wall. Due to the ellipticity of the Laplacian operator in the Poisson equation, these two quantities are strictly related and thus they have very similar patterns on both the rotor and the stator surfaces. The higher values occur in the tip regions close to the leading edge of both the rotor and the stator blades. The acoustic effectiveness of these pressure fluctuations, however, depends on a combination of Döppler and geometrical diffraction factors, requiring a more sophisticated analysis in order to be properly investigated.

Finally, available experimental spectra are used for a preliminary validation of the numerical results, as illustrated in Fig. (7). The noise spectra computed at 0 deg

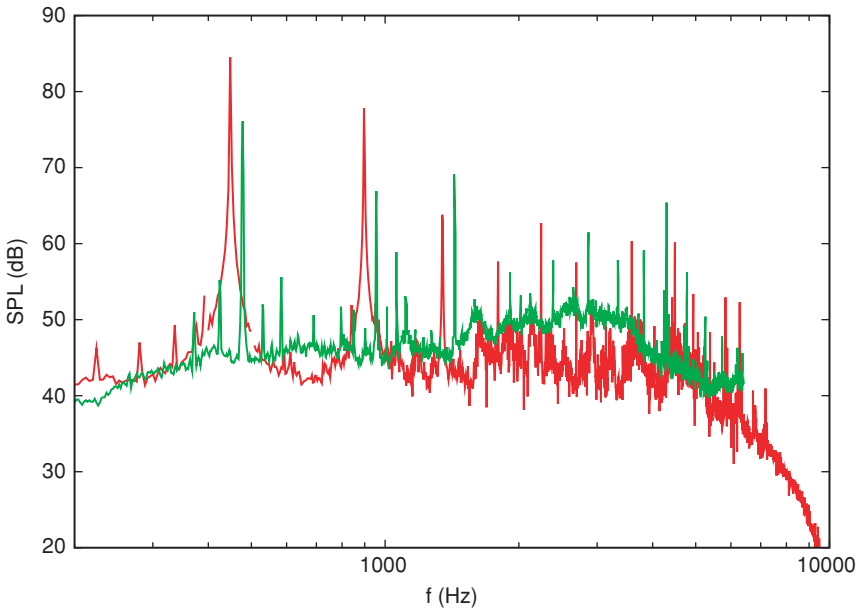

Figure 7: Comparison between experimental data and numerical results. Sound pressure levels at 0 deg (integration band 4 Hz for the numerical results and 2 Hz for the experimental data, $p_{\text{ref}} = 2\mu$ Pa). Red: numerical results, green: experimental data.

observation angles are compared with experimental measurements carried out by VALEO. A remarkable difference arise in the spectral tonal components. In fact, the experimental spectrum present several peaks around each BPF tones at multiples of the rotation frequency of 50 Hz. This phenomenon reveals the presence of low order wall pressure unsteadiness, due to spurious mock-up vibrations and to the non-uniform circumferential spacing of the rotor blades. The corresponding wall pressure Fourier components are projected into the far-field noise spectrum with a classical bell shape, as resulting from the Döppler effects in a rotating device. Conversely, the numerical results present only BPF peaks. Moreover, the predicted noise peak levels are significantly higher than the experimental ones (8–9 dB). A better global agreement can be observed for the broadband spectral components. The levels are fairly well predicted throughout the frequency range where the stochastic noise generation model is active ($f \gtrsim$ 1000 Hz). The underestimation around 3 kHz is probably due to a lack of Fourier components in the SNGR method, but this requires further investigations. Unfortunately, the addressed case study is characterized by broadband noise levels that are only about 10 dB higher than the background noise levels. Therefore, it does not allow to deeply stress and validate the present broadband noise stochastic approach.

5. CONCLUSIONS AND OUTLOOK

A stochastic method derived from the SNGR approach among "one hundred thousand methods" have been outlined and applied in this paper to predict the noise generated by a real low-speed axial fan system. The novelty of the method consists in using the SNGR approach to compute the right-hand side of a Poisson equation that is solved through a BEM approach for the wall pressure fluctuations. These are finally fed into a FW-H acoustic analogy computation that provides the noise signals at prescribed microphone locations.

The main theoretical drawback of the method is that, since the Poisson equation is based on the incompressibility hypothesis, it is not adequate to represent pressure fluctuations induced by turbulent fluctuations with supersonic phase velocity. The effect of this modeling simplification have not been investigated in this study and will be the objective of future studies.

Although the Poisson equation can be solved in a much more effcient way than the Curle's equation, which involves evaluations of the source term at retarded times and requires a more complex software structure, the main computational drawback of the present method is its computational cost in terms of both CPU time and memory occupation. A field approach will be assessed in the future as an alternative to the BEM approach.

The present application study has not revealed appreciable benefits produced by the stochastic model: the noise spectral components associated with the stochastic fluctuations fall in the high frequency regime and exhibit very low levels. However, the situation can be different with a different cooling system and with a different CFD solution. Many aspects related to the physical reliability of the model and its sensitivity to the accuracy of the RANS solution will be addressed in the future through a more rigorous validation process.

The main advantages of the method are its simplicity and the possibility to be used in connection with an integral FW-H code. In addition, similarly to other stochastic methods, it allows to compute transient solutions of long duration, enabling averaged spectral computations as in the experimental acquisition. Finally, a possible advantage of the method to be explored in the future is its direct implementation into a CFD code as an additional scalar equation for the pressure fluctuation weakly coupled with the RANS equation system.

ACKNOWLEDGMENTS

The idea of using the title "*Uno, nessuno, cento mila*" of the notorious tale by the twenty century Italian dramatist and novelist Luigi Pirandello, was inspired by Prof. Michele Ciavarella of Polytechnic University of Bari, acknowledged for that, who recently published a review article dealing with the crack propagation.

REFERENCES

[1] Moreau, S., D., M. H., and Neal, "Detailed 3D Unsteady Rotor-Stator Interaction in Automotive Engine Cooling Fan Systems," *6th European Conference on Turbomachinery Fluid Dynamics and Thermodynamics, Lille*, Mar 2005.

[2] Moreau, S. and Bakir, F., "Aeroacoustic Characteristics of Efficient Automotive Engine Cooling Fan Systems," *FEDSM2004-56824 paper*, July 2004.

[3] Carolus, T., Schneider, M., and Reese, H., "Axial Flow fan Broad-Band Noise and Prediction," *Journal of Sound and Vibration*, Vol. 300, No. 1-2, 2006, pp. 50–70.

[4] Schlinker, R. H. and Amiet, R. K., "Helicopter Trailing Edge Noise," *NASA CR-3470*, 1981.

[5] Paterson, R. W. and Amiet, R. K., "Noise of a Model Helicopter Rotor Due to Ingestion of Turbulence," *NASA CR-3213*, 1979.

[6] Moreau, S. and Roger, M., "Competing Broadband Noise Mechanisms in Low-Speed Axial Fans," *AIAA Journal*, Vol. 45, No. 1, 2007, pp. 48–57.

[7] Ffowcs Williams, J. E. and Hall, L. H., "Aerodynamic Sound Generation by Turbulent Flow in the Vicinity of a Scattering Half-Plane," *Journal of Fluid Mechanics*, Vol. 40, 1970, pp. 657–670.

[8] Chase, D. M., "Noise Radiated from an Edge in Turbulent Flow," *AIAA Journal*, Vol. 13, No. 8, 1975, pp. 1041–1047.

[9] Amiet, R. K., "Acoustic Radiation from an Airfoil in a Turbulent Stream," *Journal of Sound and Vibration*, Vol. 41, No. 4, 1975, pp. 407–420.

[10] Amiet, R. K., "Noise Due to Turbulent Flow Past a Trailing Edge," *Journal of Sound and Vibration*, Vol. 47, No. 3, 1976, pp. 387–393.

[11] Howe, M. S., "The Influence of Vortex Shedding on The Generation of Sound by Convected Turbulence," *Journal of Fluid Mechanics*, Vol. 76, No. 4, 1976, pp. 711–740.

[12] Amiet, R. K., "Effect of the Incident Surface Pressure Field on Noise Due to a Turbulent Flow Past a Trailing Edge," *Journal of Sound and Vibration*, Vol. 57, No. 2, 1978, pp. 305–306.

[13] Howe, M. S., "A Review of the Theory of Trailing-Edge Noise," *Journal of Sound and Vibration*, Vol. 61, No. 3, 1978, pp. 437–465.

[14] Howe, M. S., "Trailing Edge Noise at Low Mach-Numbers," *Journal of Sound and Vibration*, Vol. 225, No. 2, 1999, pp. 211–238.

[15] Roger, M. and Moreau, S., "Broadband Self-Noise from Loaded Fan Blades," *AIAA Journal*, Vol. 42, No. 3, 2004, pp. 536–544.

[16] Roger, M. and Moreau, S., "Bach-Scattering Correction and Further Extensions of Amiet's Trailing Edge Noise Model, Part 1: Theory," *Journal of Sound and Vibration*, Vol. 286, No. 3, 2005, pp. 477–506.

[17] Moreau, S., Henner, M., Casalino, D., Gullbrand, J., Iaccarino, G., and Wang, M., "Toward the Prediction of Low-Speed Fan Noise," *Center for Turbulence Research, Proceedings of the Summer Program 2006*, 2006, pp. 519–531.

[18] Moreau, S. and Roger, M., "Effect of Airfoil Aerodynamic Loading on Trailing Edge Noise Sources," *AIAA Journal*, Vol. 43, No. 1, 2005, pp. 41–52.

[19] Béchara, W., Bailly, C., and Candel, P. L. S., "Stochastic Approach to Noise Modeling for Free Turbulent Flows," *AIAA Journal*, Vol. 32, No. 3, 1994, pp. 455–464.

[20] Bailly, C., Lafon, P., and Candel, S., "A Stochastic Approach to Compute Noise Generation and Radiation of Free Turbulent Flows," *AIAA Paper 95-092-1-6*, 1995.

[21] Casalino, D. and Jacob, M., "Prediction of Aerodynamic Sounds from Circular Rods via Spanwise Statistical Modeling," *Journal of Sound and Vibration*, Vol. 262, No. 4, 2003, pp. 815–844.

[22] Ewert, R., "CAA Slat Noise Studies Applying Stochastic Sound Sources Based On Solenoidal Digital Filters," *AIAA Paper 2005-2862*, 2005.

[23] Ffowcs Williams, J. E., "Surface-Pressure Fluctuations Induced by Boundary-Layer Flow at Finite Mach Number," *Journal of Fluid Mechanics*, Vol. 22, No. 3, 1965, pp. 507–519.

[24] Ffowcs Williams, J. E., "Boundary-Layer Pressures and the Corcos Model: a Development to Incorporate Low-Wavenumber Constraints," *Journal of Fluid Mechanics*, Vol. 125, 1982, pp. 9–25.

[25] Curle, N., "The Influence of Solid Boundaries upon Aerodynamic Sound," *Proceeding of The Royal Society of London A*, Vol. A231, 1955, pp. 505–514.

[26] Corcos, G. M., "The Structure of a Turbulent Pressure Field in Boundary-Layer Flows," *Journal of Fluid Mechanics*, Vol. 18, 1964, pp. 353–378.

[27] Shubert, G. and Corcos, G. M., "The Dynamics of Turbulence near a Wall According to a Linear Model," *Journal of Fluid Mechanics*, Vol. 29, No. 1, 1967, pp. 113–135.

[28] Landahl, M. T., "A Wave-Guide Model for Turbulent Shear Flow," *Journal of Fluid Mechanics*, Vol. 29, No. 3, 1967, pp. 441–459.

[29] Ciskowski, R. D. and Brebbia, C. A., *Boundary Element Methods in Acoustics*, WIT Press, 1991.

[30] Press, W. H., Teukolsky, S. A., Vetterling, W. T., and Flannery, B. P., *Numerical Recipes in Fortran 77: The Art of Scientific Computing,* Vol. 1 of Fortran Numerical Recipes, Cambridge University Press, 2nd ed., 1997.

[31] Moreau, S. and Bakir, F., "Detailed Study of an Efficient Small Diameter Automotive Engine Cooling Fan System," *FEDSM2003-45117 paper*, July 2003.

[32] Henner, M., Moreau, S., Stanciu, M., Aubert, S., and Ferrand, P., "Unsteady Rotor-Stator Interactions in Automotive Engine Cooling Fan Systems," *ISUAAAT 2000* , Sep 2000.

[33] Moreau, S., Aubert, S., and Ferrand, P., "Detailed 2D Unsteady Rotor-Stator Interaction in Automotive Engine Cooling Fan Systems," *FEDSM2002-31347 paper*, July 2002.

[34] Coggiola, E., Dessale, B., Moreau, S., and Broberg, R., "On the use of CFD in the Automotive Engine Cooling Fan System Design," *AIAA Paper 98-0772*, Jan 1998.

[35] Neal, D., Moreau, S., Henner, M., and Foss, J., "Evaluating CFD Models of Axial Fans by Comparisons with Phase-Averaged Experimental Data," *Proceedings of the 5th Vehicle Thermal Management Systems Conference*, *VTMS5-01-89*, 2001.

[36] Menter, F. R., "Two-Equation Eddy-Viscosity Turbulence Models for Engineering Applications," *AIAA Journal*, Vol. 32, No. 8, August 1994, pp. 1598–1605.

[37] Casalino, D. and Genito, M., "Turbofan Aft Noise Predictions Based on the Lilley's Wave Model," *AIAA Journal*, Vol. 46, No. 1, 2008, pp. 84–93.

[38] Casalino, D., "An Advanced Time Approach for Acoustic Analogy Predictions," *Journal of Sound and Vibration*, Vol. 261, No. 4, 2003, pp. 583–612.

[39] Di Francescantonio, P., "A New Boundary Integral Formulation for the Prediction of Sound Radiation," *Journal of Sound and Vibration*, Vol. 202, No. 4, 1997, pp. 491–509.

[40] Brentner, K. S. and Farassat, F., "Analytical Comparison of the Acoustic Analogy and Kirchhoff Formulation for Moving Surfaces," *AIAA Journal*, Vol. 36, No. 8, 1998, pp. 1379–1386.